

Stability Verification for Bilateral Teleoperation System with Variable Time Delay

M. Sallam, A. Ramadan, M. Fanni and M. Abdellatif

Abstract—Time delay in bilateral teleoperation system was introduced as a sufficient reason to make the system unstable or certainly degrade the system performance. In this paper, simulations and experimental results of implementing p-like control scheme, under different ranges of variable time delay, will be presented to verify a certain criteria, which guarantee the system stability and position tracking. The system consists of two Phantom premium 1.5A devices. One of them acts as a master and the other acts as a slave. The study includes deriving the Phantom kinematic and dynamic model, establishing the link between the two Phantoms over Simulink in Matlab, and verifying the stability criteria with simulations and real experiments.

Keywords—bilateral teleoperation, Phantom premium 1.5, varying time delay

I. INTRODUCTION

TELEOPERATION is the process of controlling a machine or performing a task over a distance. Depending on risks and complexity of the task environment, the strategy for the teleoperation process should be selected. In case of structured work environment, autonomous system can be used to perform the task. However, in case of unstructured environment, some kind of human intervention may be required. Master/slave control is one of different approaches used to control a process or perform a task in unstructured environment over a distance. It enables the operator to perform manual tasks with no need for direct contact at the work site. In some cases, the task place is unreachable, hazardous, or in Micro-scale. Space technologies, radioactive material handling and micromanipulation are very common applications for such environments. As information about the contact force at the work side is reflected to the human operator, the system is said to be controlled bilaterally. Bilateral teleoperation system consists of two mechanical systems, the slave which is located in the work site and the master which is located in the control station. If time delay due to the communication channel exists between the master and slave, the system performance and stability may be affected. Anderson and Spong [1] pointed out

that even a small constant time delay can make bilateral systems unstable and certainly degrade the operator's intuition and performance.

Bilateral teleoperation system was firstly used, in the presence of time delay, in 1966 and the instability was apparent. This problem of instability could not be solved till 1989 when Anderson and Spong [1] presented their approach based on the passivity and scattering theory. Since that date several researchers addressed the problem of time delay in bilateral teleoperation systems. Some of them considered the constant time delay such as [2],[3],[4],[5] and others considered the varying time delay such as [6],[7],[8]. Emmanuel Nuño and et al in [8] proved that simple P-like controller can stabilize the teleoperator under variable time delays and, moreover, it provides position tracking. They presented conditions under which the velocities and position error of a non-linear teleoperator are bounded, and if the human does not move the local manipulator and the remote manipulator does not interact with the environment, then it is proved that velocities and position error converge to zero.

This paper investigated one of the presented conditions in [8] that guarantee the stability of the system in the presence of variable time delay. The condition is a relation between the feedback gains and maximum values of the time delay. The system response was checked when the stability condition is satisfied and when the stability condition is not satisfied. Our verification for the stability criteria was done using simulations and experiments on a real master/slave system which consists of two Phantom premium 1.5A devices. Phantom device was presented in several researches as a master device that has low inertia, good dynamic response, very smooth motion and low friction. Additionally, kinematic and dynamic model for the Phantom device were firstly derived. Notations of the robotics book of "Robot Modeling and Control" (Mark W. Spong and et al) is used in deriving the kinematic equations.

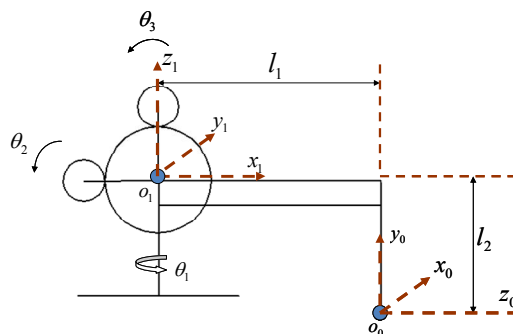


Fig. 1 Zero Configuration for the Phantom

M. Sallam is a master candidate at the Egypt-Japan University for Science and Technology, Borg-Elarab, Alexandria, Egypt (phone: 2012-033-6966; fax: 2-03-459 9520; e-mail: mohamed.sallam@ejust.edu.eg).

A. Ramadan is with the Egypt-Japan University for Science and Technology, Bourg-Elarab, Alexandria, Egypt; e-mail: ahmed.ramadan@ejust.edu.eg), on leave of Tanta University.

M. Fanni, is an associate professor with the Mansoura University, mansoura, Egypt (e-mail: mfanni@qu.edu.qa).

M. Abdellatif, is with the Egypt-Japan University for Science and Technology, Alexandria, Egypt; (e-mail: mohamed.abdellatif@ejust.edu.eg).

II. PHANTOM FORWARD KINEMATICS

Kinematic geometry of Phantom device is different from other common 3 or 6 DOF robot arms. On contrary of other types, changing the second angle θ_2 in phantom will result in changing the third angle θ_3 as well. In addition, phantom robot uses four bar mechanism to control the third angle θ_3 . Fig 1 shows a simplified drawing for the Phantom. Lengths of the manipulator links; and maximum and minimum angles of its joints are not available from the phantom company, Sensable Technologies Inc. Regarding lengths, the used values that were experimentally measured in [9], while angles boundaries, required to draw the workspace, were measured in our lab.

TABLE I
 PHANTOM LENGTHS AND ANGLES LIMITATIONS

Lengths of links	Angles limitations
$l_1 = 0.215$ m	$\theta_1 : -90$ to 90 deg,
$l_2 = 0.170$ m	$\theta_2 : -57.7$ to 115 deg,
	$\theta_3 : -25.7$ to 167.5 deg.

To describe the position and orientation for the phantom, the kinematic problem has been solved. Denavit-Hartenberg approach is used to get the final transformation matrix.

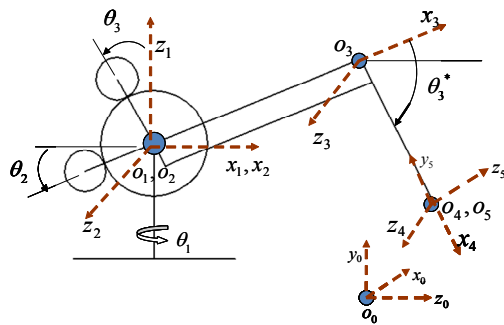


Fig. 2 Assignment of the coordinate frames

Fig 2 shows assignment of all coordinate frames. In the following steps it will be created a table of link parameters; $a_i, d_i, \alpha_i, \theta_i$. Frame 0 is considered the fixed frame. In case of describing frame 1 with respect to frame 0 and frame 4 with respect to frame 5 DH rules are not used, so the transformation matrix using the multiplication of the basic rotation matrices is calculated.

From frame 0 to frame 1

$$R = R_{y,-90} R_{x,-90} \quad , \quad T_0^1 = \begin{bmatrix} 0 & 1 & 0 & 0 \\ 0 & 0 & 1 & l_2 \\ 1 & 0 & 0 & -l_1 \\ 0 & 0 & 0 & 1 \end{bmatrix}$$

From frame 1 to frame 2

$$a_i = 0 \quad , \quad \alpha_i = 90 \quad , \quad d_i = 0 \quad , \quad \theta_i = \theta_1$$

From frame 2 to frame 3

$$a_i = l_1 \quad , \quad \alpha_i = 0 \quad , \quad d_i = 0 \quad , \quad \theta_i = \theta_2$$

From frame 3 to frame 4

$$a_i = l_2 \quad , \quad \alpha_i = 0 \quad , \quad d_i = 0 \quad , \quad \theta_i = -\theta_2 - 90 + \theta_3$$

From frame 4 to frame 5

$$R = R_{y,90} R_{x,-90} \quad , \quad T_4^5 = \begin{bmatrix} 0 & -1 & 0 & 0 \\ 0 & 0 & 1 & 0 \\ -1 & 0 & 0 & 0 \\ 0 & 0 & 0 & 1 \end{bmatrix}$$

$$T = T_0^1 T_1^2 T_2^3 T_3^4 T_4^5 \quad (1)$$

$$T = \begin{bmatrix} \cos \theta_1 & -\sin \theta_1 \sin \theta_3 & \sin \theta_1 \cos \theta_3 & \sin \theta_1 (l_2 \sin \theta_3 + l_1 \cos \theta_2) \\ 0 & \cos \theta_3 & \sin \theta_3 & -l_2 \cos \theta_3 + l_1 \sin \theta_2 + l_2 \\ -\sin \theta_1 & -\cos \theta_1 \sin \theta_3 & \cos \theta_1 \cos \theta_3 & \cos \theta_1 (l_2 \sin \theta_3 + l_1 \cos \theta_2) - l_1 \\ 0 & 0 & 0 & 1 \end{bmatrix}$$

III. PHANTOM JACOBIAN

It is seen from the transformation matrix that:

$$x = \sin \theta_1 (l_2 \sin \theta_3 + l_1 \cos \theta_2) \quad (2)$$

$$y = -l_2 \cos \theta_3 + l_1 \sin \theta_2 + l_2 \quad (3)$$

$$z = \cos \theta_1 (l_2 \sin \theta_3 + l_1 \cos \theta_2) - l_1 \quad (4)$$

$$J = \begin{bmatrix} \frac{\partial x}{\partial \theta_1} & \frac{\partial x}{\partial \theta_2} & \frac{\partial x}{\partial \theta_3} \\ \frac{\partial y}{\partial \theta_1} & \frac{\partial y}{\partial \theta_2} & \frac{\partial y}{\partial \theta_3} \\ \frac{\partial z}{\partial \theta_1} & \frac{\partial z}{\partial \theta_2} & \frac{\partial z}{\partial \theta_3} \\ Z_0 & Z_1 & Z_2 \end{bmatrix}$$

$$Z_0 = R_0^1 \begin{bmatrix} 0 \\ 0 \\ 1 \end{bmatrix}, Z_1 = R_0^1 R_1^2 * \begin{bmatrix} 0 \\ 0 \\ 1 \end{bmatrix}, Z_2 = R_0^1 R_1^2 R_2^3 * \begin{bmatrix} 0 \\ 0 \\ 1 \end{bmatrix}$$

$$J = \begin{bmatrix} \cos(\theta_1)(l_2 \sin(\theta_3) + l_1 \cos(\theta_2)) & -l_1 \sin(\theta_1) \sin(\theta_2) & l_2 \sin(\theta_1) \cos(\theta_3) \\ 0 & l_1 \cos(\theta_2) & l_2 \sin(\theta_3) \\ -\sin(\theta_1)(l_2 \sin(\theta_3) + l_1 \cos(\theta_2)) & -l_1 \cos(\theta_1) \sin(\theta_2) & l_2 \cos(\theta_1) \cos(\theta_3) \\ 0 & -\cos(\theta_1) & -\cos(\theta_1) \\ 1 & 0 & 0 \\ 0 & \sin(\theta_1) & \sin(\theta_1) \end{bmatrix}$$

Additionally, torques at the phantom joints motors due to applied forces at the end effector can be calculated by:

$$T = J^T * F \quad (5)$$

T : Torques at the phantom joints

F : Forces acting at the end effector

IV. PHANTOM DYNAMICS

Similarly to the links lengths, all masses and parameters required to build the dynamic model are not available from the

phantom company. Experimentally some researchers could measure and/or estimate all the robot dynamics and parameters as in [9] and [10]. The former has identified the phantom into seven segments from A to G. For each segment he determined the transformation matrix, calculated linear and angular velocities, derived the kinematic and dynamic energies and calculated the inertial parameters. Afterwards he used Lagrange formulation to derive the dynamic equations of the manipulator. The last aimed to experimentally identify and analyze the dynamics of the phantom device. Based on [9] the dynamic model is derived as following.

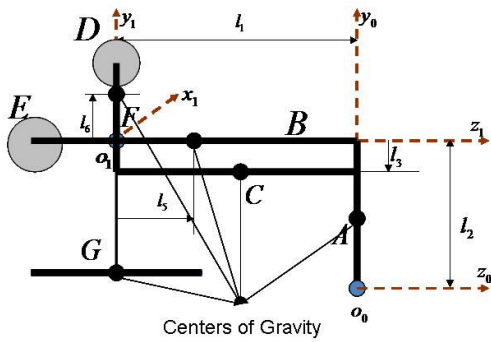


Fig. 3 Segments used in dynamic analysis

Cg_dist: distance from center of gravity to the preceding joint.

TABLE II
PHANTOM PARAMETERS

Segment A	Segment BE
$cg_dist = l_2/2 = 0.085m$	$cg_dist = l_5 = -0.0368m$
$Mass = 0.0202kg$	$Mass = 0.2359kg$
$I_{a_{xx}} = 0.4864 * 10^{-4}$	$I_{be_{xx}} = 11.09 * 10^{-4}$
$I_{a_{yy}} = 0.001843 * 10^{-4}$	$I_{be_{yy}} = 10.06 * 10^{-4}$
$I_{a_{zz}} = 0.4864 * 10^{-4}$	$I_{be_{zz}} = 0.591 * 10^{-4}$
Segment C	Segment DF
$cg_dist = l_1/2 = 0.1075m$	$cg_dist = l_6 = 0.0527m$
$Mass = 0.0249kg$	$Mass = 0.1906kg$
$I_{c_{xx}} = 0.959 * 10^{-4}$	$I_{df_{xx}} = 7.11 * 10^{-4}$
$I_{c_{yy}} = 0.959 * 10^{-4}$	$I_{df_{yy}} = 0.629 * 10^{-4}$
$I_{c_{zz}} = 0.0051 * 10^{-4}$	$I_{df_{zz}} = 6.246 * 10^{-4}$
Segment G	
$I_{base_{yy}} = 0.629 * 10^{-4}$	

Equations of Motion

- V: Potential energy.
- T: Kinetic energy.
- L: Lagrangian

$$L = T - V$$

$$L = (T_a + T_c + T_{be} + T_{df} + T_{base}) - (V_a + V_c + V_{be} + V_{df} + V_{base}) \quad (6)$$

$$\frac{d}{dt} \frac{\partial L}{\partial \theta_i'} - \frac{\partial L}{\partial \theta_i} = \tau_i, \quad i = 1, 2, 3$$

$$M(\theta)\theta'' + C(\theta, \theta')\theta' + N(\theta) = \tau$$

$$\begin{bmatrix} M_{11} & 0 & 0 \\ 0 & M_{22} & M_{23} \\ 0 & M_{32} & M_{33} \end{bmatrix} \begin{bmatrix} \theta_1'' \\ \theta_2'' \\ \theta_3'' \end{bmatrix} + \begin{bmatrix} C_{11} & C_{12} & C_{13} \\ C_{21} & 0 & C_{23} \\ C_{31} & C_{32} & 0 \end{bmatrix} \begin{bmatrix} \theta_1' \\ \theta_2' \\ \theta_3' \end{bmatrix} + \begin{bmatrix} 0 \\ N_2 \\ N_3 \end{bmatrix} = \begin{bmatrix} \tau_1 \\ \tau_2 \\ \tau_3 \end{bmatrix} \quad (7)$$

$$M_{11} = \frac{1}{8} (4I_{a_{yy}} + 4I_{a_{zz}} + 8I_{base_{yy}} + 4I_{be_{yy}} + 4I_{be_{zz}} + 4I_{c_{yy}} + 4I_{c_{zz}} + 4I_{df_{yy}} + 4I_{df_{zz}} + 4l_1^2 m_a + l_2^2 m_a + l_1^2 m_c + 4l_3^2 m_c) + \frac{1}{8} (4I_{be_{yy}} - 4I_{be_{zz}} + 4I_{c_{yy}} - 4I_{c_{zz}} + l_1^2 (4m_a + m_c)) \cos(2\theta_2) + \frac{1}{8} (4I_{a_{yy}} - 4I_{a_{zz}} + 4I_{df_{yy}} - 4I_{df_{zz}} - l_2^2 m_a - 4l_3^2 m_c) \cos(2\theta_3) + l_1 (l_2 m_a + l_3 m_c) \cos(\theta_2) \sin(\theta_3)$$

$$M_{22} = \frac{1}{4} (4I_{be_{xx}} + I_{c_{xx}} + l_1^2 m_a) + l_1^2 m_c$$

$$M_{23} = -\frac{1}{2} l_1 (l_2 m_a + l_3 m_c) \sin(\theta_2 - \theta_3)$$

$$M_{32} = M_{23}$$

$$M_{33} = \frac{1}{4} (4I_{a_{xx}} + 4I_{df_{xx}} + l_2^2 m_a + 4l_3^2 m_c)$$

$$C_{11} = \frac{1}{8} (-2\sin(\theta_2)) ((4I_{be_{yy}} - 4I_{be_{zz}} + 4I_{c_{yy}} - 4I_{c_{zz}} + 4l_1^2 m_a + l_1^2 m_c) \cos(\theta_2) + 2l_1 (l_2 m_a + l_3 m_c) \sin(\theta_3)) \theta_2 + 2\cos(\theta_3) (2l_1 (l_2 m_a + l_3 m_c) \cos(\theta_2) + (-4I_{a_{yy}} + 4I_{a_{zz}} - 4I_{df_{yy}} + 4I_{df_{zz}} + l_2^2 m_a + 4l_3^2 m_c) \sin(\theta_3)) \theta_3'$$

$$C_{12} = -\frac{1}{8} ((4I_{be_{yy}} - 4I_{be_{zz}} + 4I_{c_{yy}} - 4I_{c_{zz}} + l_1^2 (4m_a + m_c)) * \sin(2\theta_2) + 4l_1 (l_2 m_a + l_3 m_c) \sin(\theta_2) \sin(\theta_3)) \theta_1'$$

$$C_{13} = -\frac{1}{8} (-4l_1 (l_2 m_a + l_3 m_c) \cos(\theta_2) \cos(\theta_3) - (-4I_{a_{yy}} + 4I_{a_{zz}} - 4I_{df_{yy}} + 4I_{df_{zz}} + l_2^2 m_a + 4l_3^2 m_c) \sin(2\theta_3)) \theta_1'$$

$$C_{21} = -C_{12}$$

$$C_{23} = \frac{1}{2} l_1 (l_2 m_a + l_3 m_c) \cos(\theta_2 - \theta_3) \theta_3'$$

$$C_{31} = -C_{13}$$

$$C_{32} = \frac{1}{2} l_1 (l_2 m_a + l_3 m_c) \cos(\theta_2 - \theta_3) \theta_2'$$

$$N_2 = \frac{1}{2} g (2l_1 m_a + 2l_3 m_{be} + l_1 m_c) \cos(\theta_2)$$

$$N_3 = \frac{1}{2} g (l_2 m_a + 2l_3 m_c - 2l_6 m_{df}) \sin(\theta_3)$$

V. PHANTOM CONTROL

In the last section the equations of motion were derived for the Phantom device, describing the relation between the torque at each joint and the angles. In this section the Phantom Simulink model used to build our bilateral control system will be discussed. The real Phantom device accepts two types of reference inputs; torque at each joint or forces at the end effector in the three Cartesian coordinates x, y and z. In case of using the torque as an input to the Phantom the angles are

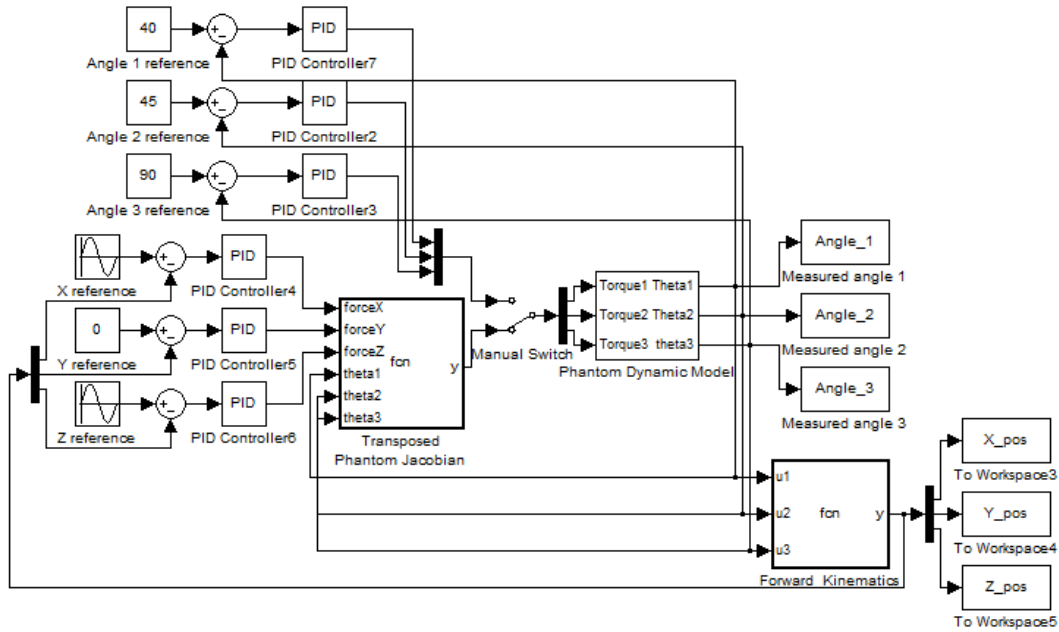


Fig. 4 Simulink block diagram for only one Phantom device control

used as controlled variables. In case of using the forces at the end effector as an input the Cartesian coordinates x , y and z should be used as controlled variables. Fig 4 shows the Simulink block diagram for one Phantom device. It is seen in the middle there is a block diagram that represents the Phantom dynamic equations. In case of making control on the robot angles, this block receives its inputs directly from the angles controllers. Assume the proportional gain is K_i and both integral and derivative gains equal Zero, then the control law will become:

$$\tau_i = K_i (q_{i_{ref}} - q_{i_{meas}}) \quad i=1,2,3 \quad (8)$$

Where;

- τ_i : The input torque to the joint (i).
- K_i : The proportional gains.
- $q_{i_{ref}}$: The reference angles
- $q_{i_{meas}}$: The measured angles

In case of using the end effector position as a reference, the Phantom dynamic model block will receive its inputs from the block of the Transposed Phantom Jacobian. The input of this block is the Cartesian forces at the end effector and its output is the equivalent torque at each joint. Equation (5) shows the function of the Transposed Phantom Jacobian block. The control law in this case will become:

$$\begin{aligned} f_x &= K_1 (X_{ref} - X_{meas}) \\ f_y &= K_2 (Y_{ref} - Y_{meas}) \\ f_z &= K_3 (Z_{ref} - Z_{meas}) \end{aligned} \quad (9)$$

Where;

- $f_{x,y,z}$: The forces at the end effector.
- X, Y, Z_{ref} : The reference position of the end effector.
- X, Y, Z_{meas} : The measured position of the end effector.

The end effector positions can be easily estimated from the forward kinematics as shown in the block diagram fig. 4.

VI. BUILDING A MATLAB AND SIMULINK MODEL FOR THE BILATERAL CONTROL SYSTEM

In bilateral control, the reference input of the slave robot is the measured variables of the master robot and vice versa. The process begins when the human operator applies force on the master device which will start to move in the direction of the applied force. The difference between the current position of the slave robot and the new position of the master robot will create an error signal forcing the slave controller to compensate that error by moving the slave robot. That will result in position tracking from the slave to the master. In case the slave manipulator interacts with the environment, the forces due to that interaction will be reflected to the master robot causing resistance to the human operator. Fig 5 explains the signal flow between the two robots in addition to the used P-like controller. K and B are the proportional and damping gains, respectively. Fig 6 shows the Simulink block diagram of our real bilateral teleoperation system. The controlled variables will be x , y and z coordinates of the Phantom end effector. As seen, the Simulink model consists mainly two blocks; one represents the master and the other represents the slave. Each of them contains the phantom dynamic model, explained in fig 4, which receives forces as inputs and give the end effector position x , y and z as outputs. Between the master

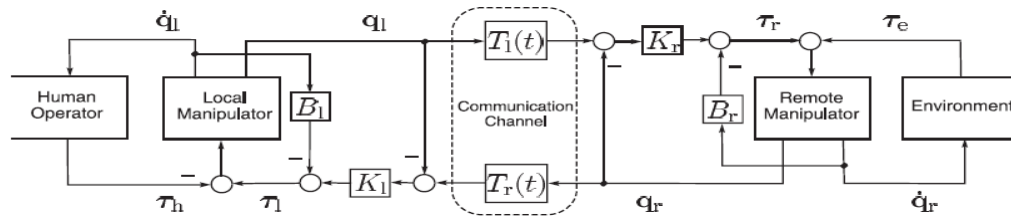


Fig. 5 P-like controller with K, B the proportional and damping gains, respectively

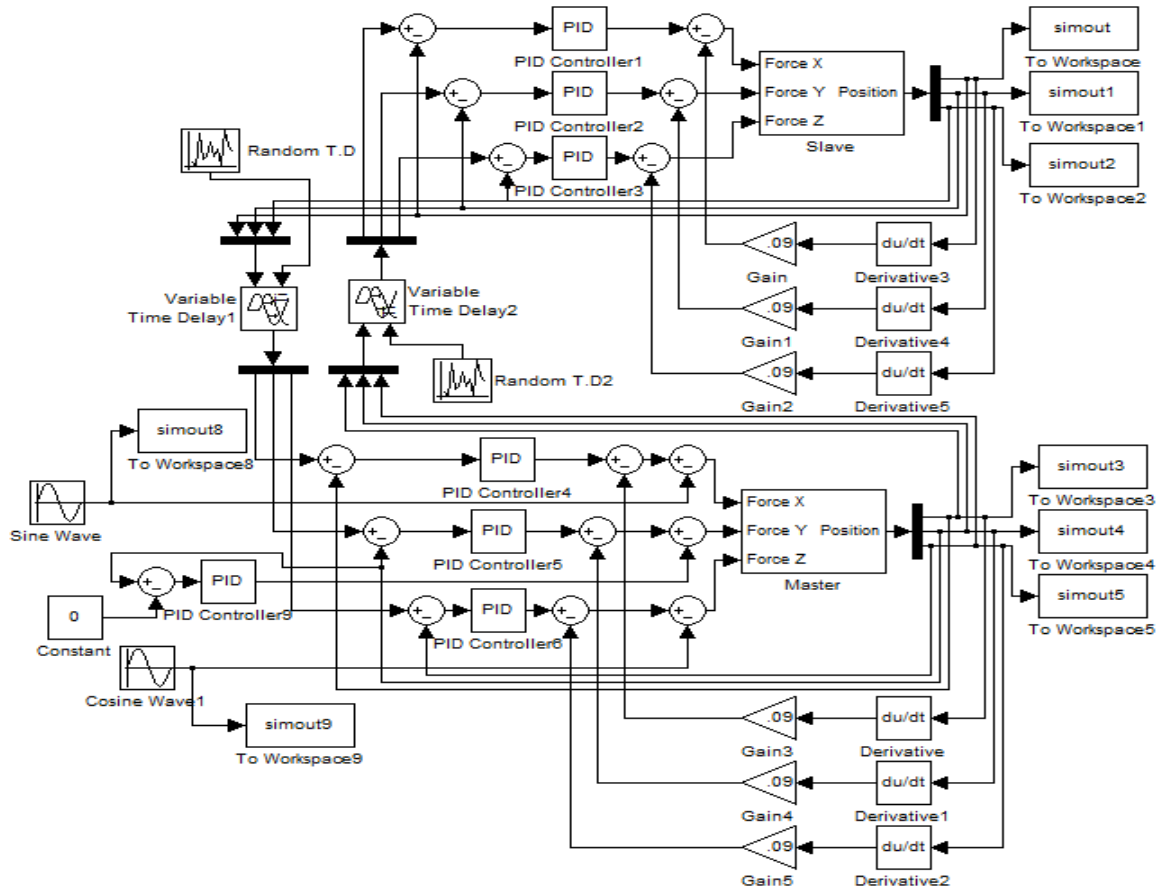


Fig. 6 Simulink block diagram of a bilateral teleoperation system

and slave blocks exists the module of the variable time delay. In this section it is implemented a P-like controller with selected suitable proportional and damping gains to investigate the validity of the stability condition used in [8]. According to the stability condition, the control gains are set such that

$$4B_m B_s > (*T_m^2 + *T_s^2) K_m K_s \quad (10)$$

B_m, B_s : The damping gains for the master and slave.

K_m, K_s : The proportional gains for the master and slave.

$*T_m, *T_s$: Max. Delay from the master to slave and vice versa.

The gains used are $K_m = K_s = 0.25$ and $B_m = B_s = 0.09$.

Assume the time delay in both directions is equal, $*T_m = *T_s$.

So if the maximum value of the time delays less than half

second, then the stability condition (10) is satisfied. Fig 8 shows the time delay used in simulation. Figures 9(a) and 11(a) show how the response is stable in simulation and experiments. If the maximum value of the time delays greater than half second, then the stability condition (10) is not satisfied. Figures 9(b) and 11(b) show how the response is not stable in simulation and experiments, with 0.6 second delay.



Fig. 7 bilateral teleoperation system using two Phantoms

In the Simulation based investigation, sine wave is used as an alternative to the human operator. In some cases when the stability condition was not satisfied, the system did not become unstable, but only the tracking was very bad.

VII. SIMULATION RESULTS

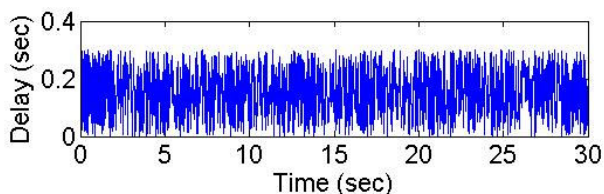
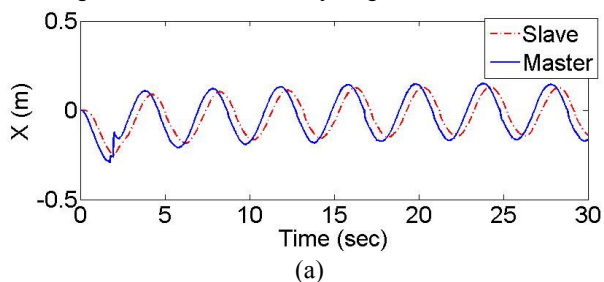
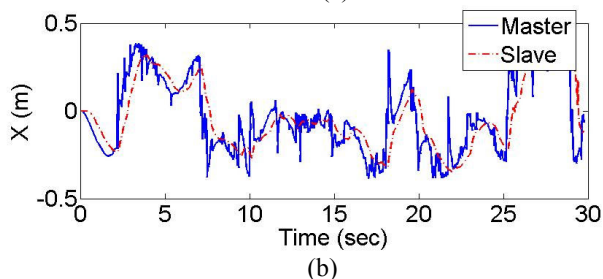


Fig. 8 the variable time delay ranges from 0 to 0.3 sec



(a)



(b)

Fig. 9 the position tracking for the simulation model in the presence of varying time delay, (a) when the stability condition is satisfied, (b) when the stability condition is not satisfied

VIII. EXPERIMENTAL RESULTS

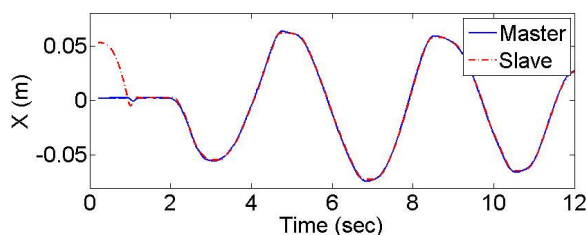
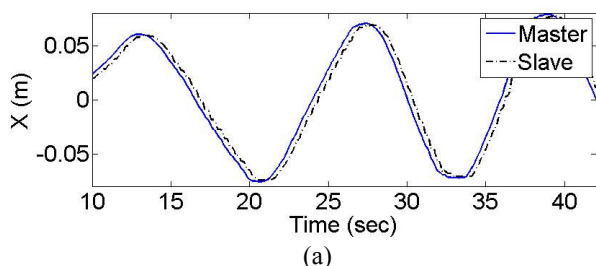
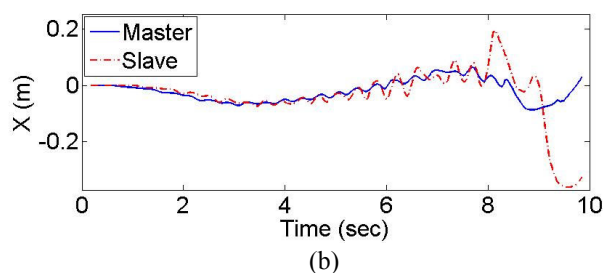


Fig. 10 the position tracking for our bilateral teleoperation system at no time delay



(a)



(b)

Fig. 11 the position tracking for the real system in the presence of varying time delay, (a) when the stability condition is satisfied, (b) when the stability condition is not satisfied

IX. CONCLUSION

In this paper we recorded our simulation and experimental results of verifying a stability condition for a bilateral teleoperation system. It has been shown that simple P-like controller, with suitable selected gains, could achieve stability in the presence of variable time delay. Additionally, the Phantom dynamic model and the Simulink block diagrams necessary to simulate and control the bilateral teleoperation system have been described. However, stability satisfaction is not enough to ensure good tracking. Work should be done to guarantee both stability and good tracking performance.

ACKNOWLEDGMENT

The authors would like to thank Egyptian missions department and Japan Cooperation Agency for their financial support.

REFERENCES

- [1] Anderson, R. and Spong, M, "Bilateral control of teleoperators with time delay," *IEEE Transactions on Automatic Control*, vol. 34, no. 5, pp. 494–501, May 1989.
- [2] Niemeyer, G. and Slotine, J., "Stable adaptive teleoperation," *IEEE Journal of Oceanic Engineering*, vol. 16, no. 1, pp. 152–162, 1991.
- [3] Hastrudi-Zaad, K. and Salcudean, S.E, "On the Use of Local Force Feedback for Transparent Teleoperation," in *Proc. 1999 IEEE Int. Conf. Rob. & Auto.*, pp. 1863–1869.
- [4] Azorin, J. M., Reinoso, O., Sabater, J. M., Perez, C., and Aracil, R., "A New Control Method of Teleoperation with Time Delay," *Int. Conf. Advanced Robotics*, Coimbra, Portugal, pp. 100-105, July 2003.
- [5] Lee, D. and Spong, M, "Passive bilateral teleoperation with constant time delay," *IEEE Transactions on Robotics*, vol. 22, no. 2, pp. 269–281, 2006.
- [6] J. H. Park and H. C. Cho, "Sliding-Mode Controller for Bilateral Teleoperation with Varying Time Delay," in *Proc. 1999 IEEWASME, Int. Conf. Advanced intelligent Mechatronics*, Atlanta, USA, pp. 19-23, September 1999.
- [7] Lozano, R., Chopra, N. and Spong, M., "Passivation of force reflecting bilateral teleoperators with time varying delay," in *Proc. Mechatronics '02*, Entschede, The Netherlands, pp. 24–26, 2002.
- [8] Nuno, E., Basañez, L., Ortega, R., and Spong, M., "Position Tracking for Non-linear Teleoperators with Variable Time Delay," in *Proc. of I. J. Robotic Res.*, 2009, pp. 895-910.
- [9] Cavusoglu M C, and Feygin D., "Kinematics and Dynamics of Phantom(TM) Model 1.5 Haptic Interface," [R]. *Berkeley: University of California, Elec. Research Laboratory Memo M01/15*, 2001.
- [10] B. Taati, A. Tahmasebi and K. Hashtudi-Zaad, "Experimental identification and analysis of the dynamics of a PHANTOMTM Premium 1.5A haptic device," *Presence: Teleoperator & Virtual Environment*, June 2008.